

各向异性表面张力对深胞晶界面形态稳定性的影响

蒋晗 陈明文 史国栋 王涛 王自东

Effect of surface tension anisotropy on the interface morphological stability of deep cellular crystal

Jiang Han Chen Ming-Wen Shi Guo-Dong Wang Tao Wang Zi-Dong

引用信息 Citation: *Acta Physica Sinica*, 65, 096803 (2016) DOI: 10.7498/aps.65.096803

在线阅读 View online: <http://dx.doi.org/10.7498/aps.65.096803>

当期内容 View table of contents: <http://wulixb.iphy.ac.cn/CN/Y2016/V65/I9>

您可能感兴趣的其他文章

Articles you may be interested in

BCC 枝晶生长原子堆垛过程的晶体相场研究

Investigation of atom-attaching process of three-dimensional body-center-cubic dendritic growth by phase-field crystal model

物理学报.2015, 64(2): 028102 <http://dx.doi.org/10.7498/aps.64.028102>

晶体相场法研究晶粒缩小过程中的位错湮灭与晶界迁移

Phase-field crystal method investigated the dislocation annihilation and grain boundary migration in grain shrink process

物理学报.2014, 63(12): 128101 <http://dx.doi.org/10.7498/aps.63.128101>

各向异性表面张力对定向凝固中深胞晶生长的影响

Effect of anisotropic surface tension on deep cellular crystal growth in directional solidification

物理学报.2014, 63(3): 038101 <http://dx.doi.org/10.7498/aps.63.038101>

双边扩散枝晶生长的定量相场模型

Quantitative phase-field model for dendritic growth with two-sided diffusion

物理学报.2012, 61(22): 228102 <http://dx.doi.org/10.7498/aps.61.228102>

基于改进元胞自动机模型的三元合金枝晶生长的数值模拟

Simulation of dendritic growth for ternary alloys based on modified cellular automaton model

物理学报.2012, 61(10): 108101 <http://dx.doi.org/10.7498/aps.61.108101>

各向异性表面张力对深胞晶界面形态稳定性的影响

蒋晗¹⁾ 陈明文^{2)†} 史国栋¹⁾ 王涛¹⁾ 王自东^{1)‡}

1)(北京科技大学材料科学与工程学院, 北京 100083)

2)(北京科技大学数理学院, 北京 100083)

(2016年1月7日收到; 2016年2月1日收到修改稿)

应用匹配渐近展开法和多变量展开法研究各向异性表面张力对定向凝固中深胞晶界面形态稳定性的影响, 通过寻找定向凝固系统的模式解获得了深胞晶界面形态满足的量子化条件. 结果表明, 与各向同性的定向凝固系统中深胞晶界面形态稳定性比较, 考虑各向异性表面张力的定向凝固中深胞晶生长界面形态也有两种整体不稳定性机制: 整体波动不稳定性 and 低频不稳定性. 随着各向异性表面张力的增加, 中性模式产生强振荡的枝晶结构的整体波动不稳定性不稳定的区域减小, 中性模式产生弱振荡的胞晶结构的低频不稳定性不稳定的区域增加.

关键词: 定向凝固, 各向异性表面张力, 深胞晶, 整体不稳定性

PACS: 68.70.+w, 81.10.Aj, 81.30.Fb

DOI: 10.7498/aps.65.096803

1 引言

在定向凝固过程中, 随着凝固速度的增加, 固-液界面形态由低速生长的平直界面依次演变为小振幅的胞晶界面^[1,2]、大振幅的深胞晶界面、枝晶界面、细胞晶界面, 再演化为高速生长的平直界面. 不论是哪种固液界面形态, 界面形态的稳定性都是材料科学领域中十分重要的科学问题. 20世纪60年代, Mullins和Sekerka^[1,2]建立了平界面形态线性稳定性理论, 这一理论已经成为研究液-固界面形态特征的重要依据(称为M-S理论). Pelcé和Karma^[3,4]研究了固-液等温情况下胞晶生长界面形态的稳定性. Pocheau和Georgelin^[5-8]研究了Hele-Shaw生长室中胞晶形成的动力学, 发现胞晶形态的选择依赖于它的生长历史. 相对于其他界面形态的研究而言, 人们对于深胞晶界面形态的研究是薄弱的. Xu和Chen^[9,10]利用Saffmen-Taylor^[11]曲线坐标得到了深胞晶形态的近似解析

解, 研究了考虑各向同性表面张力的深胞晶生长的稳定性机制. Wang等^[12,13]研究了表面张力各向异性对定向凝固过程中初始平界面稳定性的影响, 发现表面张力各向异性的非线性效应导致定向凝固界面倾斜生长. Chen等^[14]研究了各向异性表面张力对定向凝固中深胞晶生长形态的影响, 揭示了在各向异性表面张力作用下深胞晶界面微结构形态形成的物理机制. 本文应用含有各向异性表面张力的深胞晶生长的定常解作为基态进行稳定性分析, 研究了各向异性表面张力作用下定向凝固深胞晶生长的稳定性, 揭示了各向异性表面张力对不稳定区域大小的影响.

2 定向凝固系统的数学模型

考虑样本材料细长的二元合金熔体定向凝固过程中的深胞晶生长, 凝固过程可以视为二维处理, 二元混合系统中的次组元视为稀释的杂质; 忽

† 通信作者. E-mail: chenmw@ustb.edu.cn

‡ 通信作者. E-mail: wangzidong64@126.com

略溶质在固相内的扩散; 除扩散系数外, 其他热力学性质在固相和液相内是相同的, 并且系统不存在对流. 我们假定系统的温度梯度为 G_T , 远场浓度为 C_∞ , 胞晶列的周期为 l_w . 界面各向异性为四重对称函数 $\gamma(\theta) = \gamma_0(1 + \alpha_4 \cos 4\theta)$, 其中 γ_0 为各向同性表面张力参数, θ 为界面法向量与 Oy 轴之间的夹角, α_4 为各向异性表面张力的强度. 在这里, 选取深胞晶尖端曲率半径 l_t 为长度尺度, 拉速 V 为速度尺度, $l_D = \kappa_D/V$ 为溶质扩散长度, l_t/V 为时间尺度, $\Delta H/(c_p\rho)$ 为温度尺度, C_∞ 为浓度尺度, 其中 κ_D 为溶质扩散系数, ΔH 为单位体积内固相产生的潜热, c_p 为液相比热, ρ 为熔体密度, $W = l_w/l_t$ 为主间距参数. 于是, 热传导方程、溶质扩散方程和界面上的界面方程转化为无量纲的控制方程. 进一步, 本文假定深胞晶尖端曲率半径远小于溶质扩散长度, 即 $l_t \ll l_D$, 选取 $\varepsilon = \sqrt{l_t} = \sqrt{l_c/l_t}$ 为小参数,

$$M = -\frac{mC_\infty}{\Delta H/(c_p\rho)}$$

为形态学参数, 其中 $m < 0$ 是相图中液相线的斜率,

$$G = \frac{l_D}{\Delta H/(c_p\rho)} G_T$$

为温度的量纲梯度, $\lambda_G = l_D/l_G = G/M$ 为两个长度单位之比, $l_G = -mC_\infty/G_T$, $l_c = \gamma c_p \rho T_M / (\Delta H)^2$ 为毛细管长度, T_M 为纯物质熔体温度, γ 为表面张力各向同性参数. 在实际情况下, Péclet 数也是很小的, 可写为 $Pe = \varepsilon \hat{P}e = l_t/l_D$, 这里 $\hat{P}e = O(1)$. 在 (ξ, η) 曲线坐标系下^[9], 利用 Saffman-Taylor 解构造曲线坐标系 (ξ, η) , 曲线坐标系与平面直角坐标系的关系为

$$X = \xi - \frac{2(1-\lambda_0)}{\pi} \arctan\left(\frac{\sin(\pi\xi)}{e^{\pi\eta} + \cos(\pi\xi)}\right),$$

$$Y = (2\lambda_0 - 1)\eta + \frac{(1-\lambda_0)}{\pi} \times \ln\left[\frac{(e^{\pi\eta}-1)^2 + 2e^{\pi\eta}(1+\cos(\pi\xi))}{4}\right], \quad (1)$$

其中 λ_0 是与主间距参数 W 有关的待定常数.

在曲线坐标系下, 温度场的线性分布为: $T_L = \varepsilon G(WY(\xi, \eta) - y_0)$, 其中 y_0 是坐标原点到温度为液化温度 T_L 的距离, 其中 $T_L = 0$. 则 $\varepsilon \rightarrow 0$ 时, 整体定常解在界面 $\eta = O(1)$ 附近的子区域可简化为^[14]

$$C_B(\xi, \eta, \varepsilon) = y_{*0} + \varepsilon \hat{P}e \{y_{*1} - W\lambda_G Y(\xi, \eta) + W\eta[\lambda_G - (y_{*0} - 1)]\} + \dots, \quad (2)$$

其中

$$y_{*0} = \frac{1 + \lambda_G(1 - \lambda_0)}{1 - \lambda_0(1 - \kappa)},$$

$$y_{*1} = \frac{\tau_0 W \lambda_0 \lambda_G \kappa}{1 - (1 - \kappa)\lambda_0},$$

$$\tau_0 = -(2 \ln 2)(1 - \lambda_0)/\pi,$$

$$W = \frac{\pi(1 - \lambda_0)}{2\lambda_0^2}.$$

3 线性扰动系统

将非稳态解表示为两部分之和:

$$C(\xi, \eta, t, \varepsilon) = (1) + (2)$$

$$= C_B(\xi, \eta, \varepsilon) + \tilde{C}(\xi, \eta, t, \varepsilon),$$

$$\eta_S(\xi, t, \varepsilon) = (1) + (2)$$

$$= \eta_B(\xi, \varepsilon) + \tilde{\eta}_S(\xi, t, \varepsilon). \quad (3)$$

第一部分是基态, 第二部分是扰动态, 假设初始扰动的范数 $\|\tilde{C}(\xi, \eta, 0, \varepsilon)\| = O(\delta)$, 且 $\delta \ll 1$. 将系统方程以振幅参数 $\delta \ll 1$ 进行线性化处理, 可以得到线性扰动系统, 满足控制方程:

$$\frac{\partial^2 \tilde{C}}{\partial \xi^2} + \frac{\partial^2 \tilde{C}}{\partial \eta^2} + \varepsilon W \hat{P}e \left(Y_\xi \frac{\partial \tilde{C}}{\partial \xi} + X_\xi \frac{\partial \tilde{C}}{\partial \eta} - G^2 \frac{\partial \tilde{C}}{\partial t} \right) = 0. \quad (4)$$

边界条件:

- 1) 在远场区域, 当 $\eta \rightarrow \infty$ 时, $\tilde{C} \rightarrow 0$;
- 2) 在侧壁 $\xi = \pm 1$ 上, $\frac{\partial \tilde{C}}{\partial \xi} = 0$;
- 3) 在界面 $\eta = \eta_B$ 上, Gibbs-Thomson 条件:

$$\frac{\partial C_B}{\partial \eta_B} \tilde{\eta}_S + \tilde{C}$$

$$= -\varepsilon \lambda_G W \hat{P}e \frac{\partial Y(\xi, \eta_B)}{\partial \eta_B} \tilde{\eta}_S$$

$$- \frac{\varepsilon^2}{MW} K[\eta_B] \left(-\alpha_4 B_1 \tilde{\eta}_S - \alpha_4 B_2 \frac{\partial \tilde{\eta}_S}{\partial \xi} \right)$$

$$- \frac{\varepsilon^2}{MW} \{K_1 \tilde{\eta}'_S + K_2 \tilde{\eta}''_S + \frac{\partial K[\eta_B]}{\partial \eta_B} \tilde{\eta}_S\}$$

$$\times \left[1 - \alpha_4 B_0 - \alpha_4 B_1 (\eta_B + \tilde{\eta}_S) - \alpha_4 B_2 \left(\frac{\partial \eta_B}{\partial \xi} + \frac{\partial \tilde{\eta}_S}{\partial \xi} \right) \right]. \quad (5)$$

质量守恒条件:

$$\frac{\partial^2 C_B}{\partial \eta_B^2} \tilde{\eta}_S + \frac{\partial \tilde{C}}{\partial \eta_B} - \frac{\partial \tilde{\eta}_S}{\partial \xi} \left(\frac{\partial C_B}{\partial \xi} + \frac{\partial \tilde{C}}{\partial \xi} \right)$$

$$- \frac{\partial \eta_B}{\partial \xi} \frac{\partial \tilde{C}}{\partial \xi} - \frac{\partial \eta_B}{\partial \xi} \tilde{\eta}_S \frac{\partial^2 C_B}{\partial \xi \partial \eta}$$

$$\begin{aligned}
 & -\varepsilon W \hat{P} e(1-\kappa) \left(\frac{\partial C_B}{\partial \eta_B} \tilde{\eta}_S + \tilde{C} \right) \\
 & \times \left[Y_\xi \left(\frac{\partial \eta_B}{\partial \xi} + \frac{\partial \tilde{\eta}_S}{\partial \xi} \right) - Y_\eta - G^2 \left(\frac{\partial \eta_B}{\partial t} + \frac{\partial \tilde{\eta}_S}{\partial t} \right) \right. \\
 & \left. + Y_{\xi\eta} \frac{\partial \eta_B}{\partial \xi} \tilde{\eta}_S - Y_{\eta\eta} \tilde{\eta}_S \right] - \varepsilon W \hat{P} e(1-\kappa) (C_B) \\
 & \times \left[Y_\xi \frac{\partial \tilde{\eta}_S}{\partial \xi} - G^2 \frac{\partial \tilde{\eta}_S}{\partial t} + Y_{\xi\eta} \frac{\partial \eta_B}{\partial \xi} \tilde{\eta}_S - Y_{\eta\eta} \tilde{\eta}_S \right] \\
 & + (\text{h.o.t.}) = 0, \tag{6}
 \end{aligned}$$

其中

$$\begin{aligned}
 K[\eta_B] &= K_0 + K_1 \eta'_B + K_2 \eta''_B, \\
 G(\xi, \eta_B) &= \sqrt{X_\xi^2 + Y_\xi^2}, \\
 K_0 &= -\frac{\Pi_0(\xi, \eta_B)}{G^3(\xi, \eta_B)(1 + \eta'^2_B)^{1/2}}, \\
 K_1 &= \frac{\Pi_1(\xi, \eta_B)}{G^3(\xi, \eta_B)(1 + \eta'^2_B)^{1/2}}, \\
 K_2 &= -\frac{1}{G(\xi, \eta_B)(1 + \eta'^2_B)^{3/2}}, \\
 B_0 &= \frac{(a_1 - 2a_2 \cos(\pi\xi) + a_3 \cos^2(\pi\xi))}{(a_6 + a_7 \cos(\pi\xi))^2}, \\
 B_1 &= -16\pi\lambda_0(1 - \lambda_0)^2[1 - \cos(\pi\xi)] \\
 & \quad \times [a_4 - a_5 \cos(\pi\xi)] \\
 & \quad \times (a_6 + a_7 \cos(\pi\xi))^{-3}, \\
 B_2 &= -\frac{16\lambda_0[a_4 - a_5 \cos(\pi\xi)] \sin(\pi\xi)}{(a_6 + a_7 \cos(\pi\xi))^2}, \\
 \Pi_0(\xi, \eta_B) &= Y_{\xi\xi} X_\xi - X_{\xi\xi} Y_\xi, \\
 \Pi_1(\xi, \eta_B) &= X_{\xi\xi} X_\xi + Y_{\xi\xi} Y_\xi, \\
 a_1 &= 1 - 4\lambda_0 + 8\lambda_0^3 - 4\lambda_0^4, \\
 a_2 &= 1 - 4\lambda_0 + 6\lambda_0^2 - 4\lambda_0^3, \\
 a_3 &= 1 - 4\lambda_0 + 12\lambda_0^2 - 16\lambda_0^3 + 8\lambda_0^4, \\
 a_4 &= 1 - 3\lambda_0 + 2\lambda_0^2, \\
 a_5 &= 1 - 3\lambda_0 + 4\lambda_0^2 - 2\lambda_0^3, \\
 a_6 &= 1 - 2\lambda_0 + 2\lambda_0^2, \\
 a_7 &= -1 + 2\lambda_0.
 \end{aligned}$$

4 外部区域内扰动态的多重变量渐近展开(MVE)解

为了得到系统的扰动态的渐近解, 引入快变量^[10]

$$t_+ = \frac{\sigma t}{\sqrt{\varepsilon}},$$

$$\begin{aligned}
 \eta_+ &= \frac{\Psi(\xi, \eta)}{\sqrt{\varepsilon}} = \frac{1}{\sqrt{\varepsilon}} \int_0^\eta k(\xi, \eta_1) d\eta_1, \\
 \xi_+ &= \frac{\Phi(\xi, \eta)}{\sqrt{\varepsilon}} = \frac{1}{\sqrt{\varepsilon}} \int_{\xi_0}^\xi k(\xi_1, \eta) d\xi_1. \tag{7}
 \end{aligned}$$

按照多重变量 $(\xi, \eta, \xi_+, \eta_+, t_+)$, 解可以写成如下格式:

$$\begin{aligned}
 C(\xi, \eta, t, \varepsilon) &= C_B(\xi, \eta, \varepsilon) + \tilde{C}(\xi, \eta, \xi_+, \eta_+, t_+, \varepsilon), \\
 \eta_S(\xi, t, \varepsilon) &= \eta_B(\xi, \varepsilon) + \tilde{\eta}_S(\xi, \xi_+, t_+, \varepsilon). \tag{8}
 \end{aligned}$$

有如下的渐近展开:

$$\begin{aligned}
 & \tilde{C}(\xi, \eta, \xi_+, \eta_+, t_+, \varepsilon) \\
 & \sim \varepsilon e^{t_+} [\tilde{\mu}_0(\varepsilon) \tilde{C}_0(\xi, \eta, \xi_+, \eta_+) \\
 & \quad + \varepsilon^{\frac{1}{2}} \tilde{\mu}_0(\varepsilon) \tilde{C}_1(\xi, \eta, \xi_+, \eta_+) + \dots], \\
 & \tilde{\eta}_S(\xi, \xi_+, t_+, \varepsilon) \\
 & \sim e^{t_+} [\tilde{\mu}_0(\varepsilon) \tilde{h}_0(\xi, \xi_+) + \varepsilon^{\frac{1}{2}} \tilde{\mu}_0(\varepsilon) \tilde{h}_1(\xi, \xi_+) + \dots], \\
 & k(\xi, \eta, \varepsilon) \sim k_0(\xi, \eta) + \varepsilon^{\frac{1}{2}} k_1(\xi, \eta) + \dots, \\
 & g(\xi, \eta, \varepsilon) \sim g_0(\xi, \eta) + \varepsilon^{\frac{1}{2}} g_1(\xi, \eta) + \dots, \\
 & \sigma = \sigma_0 + \varepsilon^{\frac{1}{2}} \sigma_1 + \dots. \tag{9}
 \end{aligned}$$

4.1 首阶奇异摄动展开(SPE)解

将(7)–(9)代入界面条件(4)–(6), 可以得到系统的控制方程为

$$\frac{\partial^2 \tilde{C}_0}{\partial \xi_+^2} + \frac{\partial^2 \tilde{C}_0}{\partial \eta_+^2} = 0. \tag{10}$$

边界条件:

- 1) 在远场区域, 当 $\eta_+ \rightarrow +\infty$ 时, $\tilde{C}_0 \rightarrow 0$;
- 2) 在侧壁, 当 $\xi = \pm 1$ 时, $\frac{\partial \tilde{C}_0}{\partial \xi_+} = 0$;
- 3) 在界面 $\eta = \eta_+ = 0$ 上, Gibbs-Thomson 条件

件

$$\begin{aligned}
 \tilde{C}_0 &= -\hat{P} e W (\lambda_G - y_{*0} + 1) \tilde{h}_0 \\
 & \quad + \frac{k_0^2}{M W G_0} \frac{\partial^2 \tilde{h}_0}{\partial \xi_+^2} (1 - \alpha_4 B_0). \tag{11}
 \end{aligned}$$

质量守恒条件:

$$\begin{aligned}
 k_0 \frac{\partial \tilde{C}_0}{\partial \eta_+} + k_0 \hat{P} e W \frac{\partial \tilde{h}_0}{\partial \xi_+} Y_\xi [\lambda_G - y_{*0} (1 - \kappa)] \\
 + W \hat{P} e (1 - \kappa) y_{*0} G_0^2 \sigma_0 \tilde{h}_0 = 0, \tag{12}
 \end{aligned}$$

- 4) 在胞晶尖端 $\xi = \xi_+ = 0$ 处, $\tilde{h}_0 = 0$, $\frac{\partial \tilde{h}_0}{\partial \xi_+} = 0$;

- 5) 根部条件, 当 $\xi_+ \rightarrow +\infty$ 时, $\tilde{h}_0 \rightarrow 0$.

则首阶近似有如下模式解:

$$\begin{aligned}
 \tilde{C}_0 &= \tilde{A}_0(\xi, \eta) \exp\{i\xi_+ - \eta_+\}, \\
 \tilde{h}_0 &= \tilde{D}_0 \exp\{i\xi_+\}. \tag{13}
 \end{aligned}$$

将(13)式代入(11)和(12)式可得色散公式:

$$\sigma_0 = -\frac{k_0^3(1-\alpha_4 B_0)}{\bar{A}_0 \bar{A}_1 G_0^3} + \frac{k_0 \lambda_0}{\bar{A}_0 G_0^2} + \frac{i k_0 Y_{\xi,0}}{\bar{A}_0 G_0^2}, \quad (14)$$

其中 \tilde{D}_0 为一个任意的复常数,

$$\bar{A}_0 = \frac{(1-\kappa)y_{*0}}{(1-\kappa)y_{*0} - \lambda_G} > 0,$$

$$\bar{A}_1 = M \hat{P} e W^2 [(1-\kappa)y_{*0} - \lambda_G] > 0,$$

此色散公式是 k_0 的三次多项式, 对给定的复参数 σ_0 , 可以得到三个复波数: $\{k_0^{(1)}(\xi, 0), k_0^{(2)}(\xi, 0), k_0^{(3)}(\xi, 0)\}$.

4.2 变量替换

为了进一步分析色散公式, 引用新的变量 ρ 来替代 $\xi^{[10]}$, 令

$$\rho = -\frac{Y_{\xi}(\xi, 0)}{\lambda_0} = \left(\frac{1-\lambda_0}{\lambda_0}\right) \tan\left(\frac{\pi\xi}{2}\right). \quad (15)$$

当 $\xi \rightarrow 1^-$ 时, 有 $\rho \rightarrow \infty$. 且由于 $G_0 = G(\xi, 0)$, 则

$$G_0 = \lambda_0 S(\rho), \quad P(\rho) = \frac{d\rho}{d\xi} = \frac{\pi}{2a}(\rho + ai)(\rho - ai),$$

其中 $S(\rho) = \sqrt{1 + \rho^2}$, $a = (1 - \lambda_0)/\lambda_0$.

应用新变量 ρ , 扰动态的解(13)转化为如下形式:

$$\begin{aligned} \tilde{h}_0(\xi) &= \tilde{D}_0 \exp\left\{\frac{i}{\sqrt{\varepsilon}} \int_{\rho_0}^{\rho} k(\rho_1, 0) d\rho_1\right\} \\ &= \tilde{h}_0(\rho). \end{aligned} \quad (16)$$

则色散(14)式变为

$$\begin{aligned} \sigma_0 &= \frac{k_0(\rho)P(\rho)}{\bar{A}_0 \lambda_0 S^2(\rho)} \left[-\frac{k_0^2(\rho)P^2(\rho)}{\bar{A}_1 \lambda_0^2 S(\rho)} (1 - \alpha_4 B_0) \right. \\ &\quad \left. + (1 - i\rho) \right]. \end{aligned} \quad (17)$$

其中

$$k_e(\rho) = \frac{k_0(\rho)P(\rho)}{\sqrt{\bar{A}_1} \lambda_0} \sqrt{1 - \alpha_4 B_0},$$

假设

$$\sigma_e = \frac{\bar{A}_0}{\sqrt{\bar{A}_1}} \sigma_0 \sqrt{1 - \alpha_4 B_0}.$$

则方程 σ_e 的 3 个根分别为

$$\begin{aligned} k_e^{(1)}(\rho) &= M(\rho) \cos\left\{\frac{1}{3} \cos^{-1}\left[\frac{\sigma_e}{N(\rho)}\right]\right\}, \\ k_e^{(2)}(\rho) &= M(\rho) \cos\left\{\frac{1}{3} \cos^{-1}\left[\frac{\sigma_e}{N(\rho)}\right] + \frac{2}{3}\pi\right\}, \\ k_e^{(3)}(\rho) &= M(\rho) \cos\left\{\frac{1}{3} \cos^{-1}\left[\frac{\sigma_e}{N(\rho)}\right] + \frac{4}{3}\pi\right\}, \end{aligned} \quad (18)$$

其中

$$M^2(\rho) = \frac{4}{3} S(\rho)(1 - i\rho),$$

$$N(\rho) = -\frac{M(\rho)(1 - i\rho)}{3S^2(\rho)}.$$

要使浓度场满足远离界面的远场条件 $\tilde{C}_0 \rightarrow 0$, $\text{Re}\{k_0(\xi, 0)\} > 0$ 是必须的, 则只有 $H_1(\rho)$ 和 $H_3(\rho)$ 有意义. 从而, 外部区域的通解可用两个基本界面行波的组合表示:

$$\begin{aligned} \tilde{h}_0(\rho) &= D_1 \exp\left\{\frac{i}{\sqrt{\varepsilon}} \int_{\rho_0}^{\rho} [k_0^{(1)}(\rho_1, 0) \right. \\ &\quad \left. + \varepsilon k_1^{(1)}(\rho_1, 0) + \dots] d\rho_1\right\} \\ &\quad + D_3 \exp\left\{\frac{i}{\sqrt{\varepsilon}} \int_{\rho_0}^{\rho} [k_0^{(3)}(\rho_1, 0) \right. \\ &\quad \left. + \varepsilon k_1^{(3)}(\rho_1, 0) + \dots] d\rho_1\right\}, \end{aligned} \quad (19)$$

常数 D_1 和 D_3 待定, 且在复平面 ρ 上沿 ρ 的实轴为分片常数.

5 奇异点 $(\varsigma_c, 0)$ 附近的内解

由于 MVE 解在扩展 (ς, η) 平面内的 $(\varsigma_c, 0)$ 处不再有效, 这表示解在 $(\varsigma_c, 0)$ 的邻域 ($|\varsigma - \varsigma_c| \ll 1; |\eta| \ll 1$) 内不再有多个长度尺度. 因此, 为求点 $(\varsigma_c, 0)$ 附近的内解, 需要引入内变量^[10]

$$\varsigma_* = \frac{\varsigma - \varsigma_c}{\varepsilon^\alpha}, \quad \eta_* = \frac{\eta}{\varepsilon^\alpha}, \quad (20)$$

指数 α 待定. 则界面形状函数变为 $\tilde{\eta}_S(\varsigma, t, \varepsilon) = \varepsilon^\alpha \tilde{\eta}_{*S}(\varsigma_*, t_+, \varepsilon)$, 杂质浓度为 $\tilde{C}(\varsigma, \eta, t, \varepsilon) = \varepsilon^\alpha \tilde{C}_*(\varsigma_*, \eta_*, t_+, \varepsilon)$. 有以下渐近展开:

$$\begin{aligned} &\tilde{C}_*(\varsigma_*, \eta_*, t_+, \varepsilon) \\ &= \varepsilon [\tilde{v}_0(\varepsilon) \tilde{C}_{*0}(\varsigma_*, \eta_*) + \tilde{v}_1(\varepsilon) \tilde{C}_{*1}(\varsigma_*, \eta_*) + \dots] e^{t_+}, \\ &\quad \tilde{\eta}_{*S}(\varsigma_*, t_+, \varepsilon) \\ &= [\tilde{v}_0(\varepsilon) \tilde{h}_{*0}(\varsigma_*) + \tilde{v}_1(\varepsilon) \tilde{h}_{*1}(\varsigma_*) + \dots] e^{t_+}. \end{aligned} \quad (21)$$

5.1 ς_c 附近的内解的首阶近似

将(20)和(21)式代入界面条件(4)–(6), 可得内解系统首阶近似的控制方程为

$$\frac{\partial^2 \tilde{C}_{*0}}{\partial \varsigma_*^2} + \frac{\partial^2 \tilde{C}_{*0}}{\partial \eta_*^2} = 0. \quad (22)$$

边界条件:

在 $\eta_* = 0$ 处, Gibbs-Thomson 条件

$$\tilde{C}_{*0} = -\hat{P} e W [\lambda_G - (y_{*0} - 1)] \tilde{h}_{*0}$$

$$+ \frac{\varepsilon^{1-2\alpha}}{MWG_0} \frac{\partial^2 \tilde{h}_{*0}}{\partial \varsigma_*^2} (1 - \alpha_4 B_0). \quad (23)$$

质量守恒条件:

$$\frac{\partial \tilde{C}_{*0}}{\partial \eta_*} + \hat{P}eW[\lambda_G - (1 - \kappa)y_{*0}]Y_\xi(\xi, 0) \frac{\partial \tilde{h}_{*0}}{\partial \varsigma_*} + \varepsilon^{\alpha-\frac{1}{2}}W\hat{P}e(1 - \kappa)y_{*0}\sigma_0G_0^2\tilde{h}_{*0} = 0. \quad (24)$$

由控制方程 (22) 以及解的解析性, 可得 $\frac{\partial \tilde{C}_{*0}}{\partial \eta_*} = i \frac{\partial \tilde{C}_{*0}}{\partial \varsigma_*}$. 假设 $\rho = -\frac{Y_\xi(\xi, 0)}{\lambda_0}$ 和 $\rho_* = \frac{\rho - \rho_c}{\varepsilon^\alpha}$, 则由界面条件 (23) 和 (24) 可得:

$$\begin{aligned} &\varepsilon^{1-2\alpha}P^3(\rho)\frac{\partial^3\tilde{h}_{*0}}{\partial\rho_*^3}(1-\alpha_4B_0) \\ &+ \bar{\Lambda}_1\lambda_0^2S(\rho)P(\rho)(1-i\rho)\frac{\partial\tilde{h}_{*0}}{\partial\rho_*} \\ &- i\varepsilon^{\alpha-\frac{1}{2}}W^2M\hat{P}e(1-\kappa)y_{*0}\sigma_0\lambda_0^3S^3(\rho)\tilde{h}_{*0} \\ &+ (\text{h.o.t}) = 0. \end{aligned} \quad (25)$$

对外部区域的解和内部区域的解分别应用变换 [10]

$$\begin{aligned} \tilde{h}_0(\rho) &= \tilde{W}_0(\rho) \exp\left\{\frac{i}{\sqrt{\varepsilon}}\int_{\rho_c}^{\rho}k_c(\rho_1)d\rho_1\right\}, \\ \tilde{h}_{*0}(\rho_*) &= \tilde{W}_{*0}(\rho_*) \exp\left\{\frac{i}{\sqrt{\varepsilon}}\int_{\rho_c}^{\rho}k_c(\rho_1)d\rho_1\right\}, \end{aligned} \quad (26)$$

波数函数 $k_c(\rho)$ 待定, 且满足 $\text{Re}\{k_0^{(3)}\} < \text{Re}\{k_c\} < \text{Re}\{k_0^{(1)}\}$. 这样外部区域的解 \tilde{h}_0 可以看作是二个 W 波的组合, 可写为

$$\tilde{W}_0(\rho) = D_1\tilde{W}_0^{(+)}(\rho) + D_3\tilde{W}_0^{(-)}(\rho), \quad (27)$$

其中

$$\begin{aligned} \tilde{W}_0^{(+)}(\rho) &= H_1(\rho) \exp\left\{-\frac{i}{\sqrt{\varepsilon}}\int_{\rho_c}^{\rho}k_c(\rho_1)d\rho_1\right\}, \\ \tilde{W}_0^{(-)}(\rho) &= H_3(\rho) \exp\left\{-\frac{i}{\sqrt{\varepsilon}}\int_{\rho_c}^{\rho}k_c(\rho_1)d\rho_1\right\}. \end{aligned}$$

把方程 (25) 重写为函数 $\tilde{W}_{*0}(\rho_*)$ 的控制方程:

$$\begin{aligned} &\varepsilon^{1-2\alpha}\Omega_3(\rho)\frac{\partial^3\tilde{W}_{*0}(\rho_*)}{\partial\rho_*^3} + \varepsilon^{\frac{1}{2}-\alpha}\Omega_2(\rho)\frac{\partial^2\tilde{W}_{*0}(\rho_*)}{\partial\rho_*^2} \\ &+ \Omega_1(\rho)\frac{\partial\tilde{W}_{*0}(\rho_*)}{\partial\rho_*} - i\varepsilon^{\alpha-\frac{1}{2}}W^2M\hat{P}e(1-\kappa)y_{*0} \\ &\times [\sigma_0 - \Omega_0(\rho)]\lambda_0^3S^3(\rho)\tilde{W}_{*0}(\rho_*) \\ &+ (\text{h.o.t}) = 0, \end{aligned} \quad (28)$$

其中

$$\begin{aligned} \Omega_3(\rho) &= P^3(\rho)(1 - \alpha_4 B_0), \quad \Omega_2(\rho) = 3ik_c\Omega_3(\rho), \\ \Omega_1(\rho) &= -3k_c^2\Omega_3(\rho) + \bar{\Lambda}_1\lambda_0^2S(\rho)P(\rho)(1 - i\rho), \\ \Omega_0(\rho) &= \sum(k_c, \varsigma) \end{aligned}$$

$$= \frac{k_c(\rho)P(\rho)}{\bar{\Lambda}_0\lambda_0S^2(\rho)} \left[-\frac{k_c^2(\rho)P^2(\rho)}{\bar{\Lambda}_1\lambda_0^2S(\rho)}(1 - \alpha_4 B_0) + (1 - i\rho) \right].$$

在此, 选取 $k_c = \sqrt{\frac{\bar{\Lambda}_1\lambda_0^2S(\rho)(1 - i\rho)}{3P^2(\rho)(1 - \alpha_4 B_0)}}$, 可以使得

$\Omega_1(\rho) = 0$, 则函数 $\tilde{W}_{*0}(\rho_*)$ 的控制方程 (28) 可以最终化为

$$\begin{aligned} &\varepsilon^{1-2\alpha}P^3(\rho)(1 - \alpha_4 B_0)\frac{\partial^3\tilde{W}_{*0}(\rho_*)}{\partial\rho_*^3} \\ &+ \varepsilon^{\frac{1}{2}-\alpha}i\lambda_0P^2(\rho)\sqrt{3\bar{\Lambda}_1S(\rho)(1 - i\rho)(1 - \alpha_4 B_0)} \\ &\times \frac{\partial^2\tilde{W}_{*0}(\rho_*)}{\partial\rho_*^2} - i\varepsilon^{\alpha-\frac{1}{2}}W^2M\hat{P}e(1 - \kappa)y_{*0} \\ &\times \left[\sigma_0 - \frac{2}{\sqrt{27(1 - \alpha_4 B_0)}}\frac{\sqrt{\bar{\Lambda}_1}(1 - i\rho)^{\frac{3}{2}}}{\bar{\Lambda}_0S^{\frac{3}{2}}(\rho)} \right] \\ &\times \lambda_0^3S^3(\rho)\tilde{W}_{*0}(\rho_*) + (\text{h.o.t}) = 0. \end{aligned} \quad (29)$$

可以发现方程 (29) 有五个孤立奇点和转向点: $\rho = \pm i, \pm i\alpha, \rho_c$. 其中 ρ_c 是复平面 ρ 内的一个简单转向点, $\rho = \pm i, \pm i\alpha$ 分别是函数 $S(\rho)$ 和 $P(\rho)$ 的零点. 由于

$$\begin{aligned} \sigma_0 &= \Omega_0(\rho_c) \\ &= \frac{2}{\sqrt{27(1 - \alpha_4 B_0)}}\frac{\sqrt{\bar{\Lambda}_1}}{\bar{\Lambda}_0}\left(\frac{1 - i\rho_c}{1 + i\rho_c}\right)^{\frac{3}{4}}, \end{aligned} \quad (30)$$

要研究转向点 ρ_c 附近内解的行为来得到一致有效渐近解, 需要考虑两种情况:

- 1) $|\sigma_0| = O(1)$; 2) $|\sigma_0| \ll 1$.

5.2 内解结果的总结

分别考虑上述两种情况, 可以得到在内部区域远离远场处的内部方程的统一形式:

$$\frac{\partial^2\tilde{W}_{*0}(\hat{\rho}_*)}{\partial\hat{\rho}_*^2} + \hat{\rho}_*^{p_0}\tilde{W}_{*0}(\hat{\rho}_*) = 0. \quad (31)$$

并且远场处内解的首阶近似具有形式:

$$\tilde{W}_{*0}(\hat{\rho}_*) = D_*\hat{\rho}_*^{\frac{1}{2}}H_v^{(2)}(z), \quad (32)$$

其中 $z = 2v\hat{\rho}_*^{\frac{1}{2v}}$, $v = \frac{1}{p_0 + 2}$.

对情形 1) $|\sigma_0| = O(1)$: $\hat{\rho}_* = A^{\frac{1}{3}}\rho_*$, $A = O(1)$, $p_0 = 1$, $\theta_L = \frac{2}{3}\pi$, $\alpha = \frac{1}{3}$, $v = \frac{1}{3}$;

对情形 2) $|\sigma_0| \ll 1$: $\hat{\rho}_* = A_*^{\frac{4}{15}}\rho_*$, $A_* = O(1)$, $p_0 = \frac{7}{4}$, $\theta_L = \frac{8}{15}\pi$, $\alpha = \frac{2}{7}$, $v = \frac{4}{15}$.

参数 θ_L 表示两条 Stokes 线之间的开角. 两种情况下的连接条件具有统一形式:

$$1) \frac{D_1}{D_3} = -i2 \cos(v\pi) = 2 \cos(v\pi) e^{-\frac{1}{2}\pi i},$$

$$D_3 = D'_3; \quad (33)$$

$$2) \frac{D_1}{D_3} = 0, \quad D_3 = D'_3. \quad (34)$$

在此基础上, 应用尖端光滑条件后, 特征值 σ_0 将会确定为稳定性参数 ε 和其他物理参数的函数.

6 整体稳定性机制

6.1 复特征值的频谱及整体振荡 (GTW) 不稳定性

首先考虑情况 1), 此时 $p_0 = 1, v = 1/3$. 假设 $\sigma_0 = \sigma_R - i\omega (\omega > 0)$. 我们只对生长速度很小的情况 ($|\sigma_R| \ll 1$) 进行稳定性分析. 在外部区域内, 使用复特征值 σ_0 表示的物理量为 $\text{Re}\{\tilde{h}_0(\rho, t)\} = \text{Re}\{H(\rho)e^{\frac{\sigma_0 t}{\sqrt{\varepsilon}}}\}$, 这里 $H(\rho) = D_1 H_1 + D_3 H_3$, 令 $d_1 = D_1 e^{-i\chi_1}, d_3 = D_3 e^{-i\chi_3}$, 其中

$$\chi_1 = \frac{1}{\sqrt{\varepsilon}} \int_0^{\rho_c} k_0^{(1)} d\rho, \quad \chi_3 = \frac{1}{\sqrt{\varepsilon}} \int_0^{\rho_c} k_0^{(3)} d\rho.$$

再根据连接条件 (33), 可得

$$\frac{d_1}{d_3} = -i e^{-i\chi}, \quad (35)$$

$$\text{其中 } \chi = \frac{1}{\sqrt{\varepsilon}} \int_0^{\rho_c} (k_0^{(1)} - k_0^{(3)}) d\rho.$$

为了满足尖端光滑性条件, 系数 d_1 和 d_3 必服从

1) 对称 S-模式,

$$\frac{d_3}{d_1} = -\frac{k_0^{(1)}(0)}{k_0^{(3)}(0)}; \quad (36)$$

2) 反对称 A-模式,

$$d_1 = -d_3. \quad (37)$$

则由 (35)–(37) 式, 可以得到量子化条件:

$$\frac{1}{\sqrt{\varepsilon}} \int_0^{\rho_c} (k_0^{(1)} - k_0^{(3)}) d\rho = \left(2n + 1 + \frac{1}{2} + \theta_0\right) \pi - i \ln \alpha_0$$

$$(n = 0, \pm 1, \pm 2, \dots), \quad (38)$$

这里 S-模式: $\alpha_0 e^{i\theta_0 \pi} = \frac{k_0^{(1)}(0)}{k_0^{(3)}(0)}$; A-模式: $\alpha_0 = 1, \theta_0 = 0$.

量子化条件 (38) 确定了复特征值 $\sigma_0 (|\sigma_0| = O(1))$ 的频谱: $\{\sigma_{0,n}\}, (n = 0, 1, 2, \dots)$, 它们是

参数 λ_0, ε 和 α_4 的函数. 此频谱产生了两个离散的本征模式列: S-模式和 A-模式. 给定 $\lambda_0, \hat{P}e$ 和其他物理参数, 系统允许一组中性稳定模式 $\sigma_R = 0$, 此时 $\varepsilon = \varepsilon_{*,n} (n = 0, 1, 2, \dots)$ 且 $\varepsilon_* = \varepsilon_{*,0} > \varepsilon_{*,1} > \varepsilon_{*,2} > \dots$. 这些模式表现为沿界面传播的行波, 所以也称此整体振荡不稳定机制为 GTW 机制. 为了方便计算, 采用新的操作参数:

$$\varepsilon_c = \sqrt{\frac{l_c V}{\kappa_D}}, \quad \lambda_G = \frac{G_c}{\varepsilon_c^2}, \quad \bar{\Lambda}_1 = \hat{P}e \hat{\Lambda}_1,$$

其中

$$G_c = \frac{l_c}{l_G}, \quad \hat{\Lambda}_1 = MW^2 \left[(1-\kappa)y_{*0} - \frac{G_c}{\varepsilon_c^2} \right], \quad \hat{P}e = \frac{\varepsilon_c^2}{\varepsilon^3}.$$

由 (18), (30) 和 (38) 式可以得到 ε_* 与 λ_0 的关系, 发现在首阶近似下, 含有各向异性表面张力时, 对于同一个 n , GTW-S 模式增长率比 GTW-A 模式更大, 这种情况我们称 GTW-S 模式比 GTW-A 模式更危险. 由图 1 可得, 在 GTW 机制下最危险的模式为 $n = 0$ 的模式. 由图 2 可得, 当各向异性表面张力参数 α_4 越大时, 系统就越稳定.

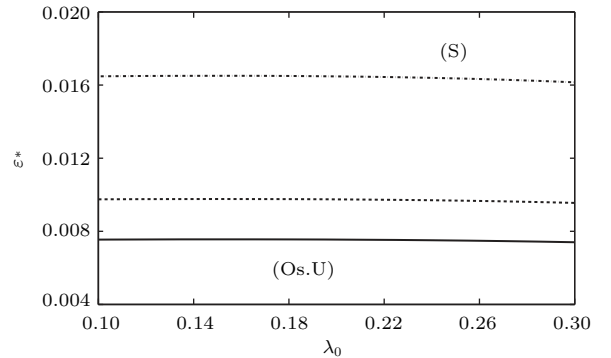


图 1 首阶近似下的 GTW-S 中性模式曲线 从上到下分别对应 $n = 0, 1, 2$, 各参数值为 $\varepsilon_c = 0.5388 \times 10^{-2}, M = 0.09552, \kappa = 0.29, G_c = 0.11485 \times 10^{-4}, \lambda_G = 0.4989, \alpha_4 = 0.1$

Fig. 1. The neutral curves of the GTW-S-modes in zeroth-order approximations for the case $\varepsilon_c = 0.5388 \times 10^{-2}, M = 0.09552, \kappa = 0.29, G_c = 0.11485 \times 10^{-4}, \lambda_G = 0.4989, \alpha_4 = 0.1$, and $n = 0, 1, 2$ from top to bottom.

从上述分析可得, GTW-S 中性模式产生强振荡枝晶结构 [10], 将参数平面 (ε, λ_0) 分成了两个区域. (S) 区域 (稳定区域) 和 (Os.U) 区域 (振荡不稳定区域). 系统的基态服从振荡稳定性判据: $(\varepsilon, \lambda_0) \in (S)$, 稳定; $(\varepsilon, \lambda_0) \in (Os.U)$, 振荡不稳定.

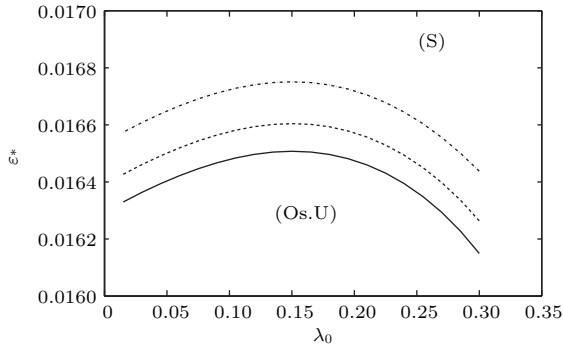


图2 首阶近似下的GTW-S中性模式曲线 ($n = 0$) 各参数值为 $\varepsilon_c = 0.5388 \times 10^{-2}$, $M = 0.09552$, $\kappa = 0.29$, $G_c = 0.11485 \times 10^{-4}$, $\lambda_G = 0.4989$, 从上到下的三条曲线分别对应 $\alpha_4 = 0, 0.06, 0.1$, 此时对应的 $\text{Re}\{\sigma_e\} = 0, 0.003, 0.005$

Fig. 2. The neutral curves of the GTW-S-modes ($n = 0$) in zeroth-order approximations for the case $\varepsilon_c = 0.5388 \times 10^{-2}$, $M = 0.09552$, $\kappa = 0.29$, $G_c = 0.11485 \times 10^{-4}$, $\lambda_G = 0.4989$, and $\alpha_4 = 0, 0.06, 0.1$, which corresponding to $\text{Re}\{\sigma_e\} = 0, 0.003, 0.005$, from top to bottom.

6.2 实特征值的频谱及低频 (LF) 不稳定性

考虑情况2). 外部区域的物理解为 $\text{Re}\{\tilde{h}(\rho, t)\} = \text{Re}\{H(\rho)\} e^{\frac{\sigma_0 t}{\varepsilon}}$, 系统允许两种类型的整体 LF 模式.

1) 对称 S-模式由此模式的尖端光滑性条件可得:

$$\begin{aligned} \text{Re}\{H(\rho)'\}(0) &= \text{Re}\{H'(0)\} \\ &= \text{Re}\left\{\frac{id_1}{\sqrt{\varepsilon}}k_0^{(1)}(0) + \frac{id_3}{\sqrt{\varepsilon}}k_0^{(3)}(0)\right\} = 0. \end{aligned} \quad (39)$$

再根据连接条件 (34) 可得:

$$\frac{d_1}{d_3} = \left|\frac{d_1}{d_3}\right| e^{-i\chi_0\pi} \quad (\chi_0 = 0, 1). \quad (40)$$

因此, 此模式下的量子化条件为

$$\begin{aligned} \text{Re}\left\{\frac{1}{\sqrt{\varepsilon}}\int_0^{\rho_c}(k_0^{(1)} - k_0^{(3)})d\rho\right\} \\ = \left(2n \pm \frac{1}{2}\right)\pi \quad (n = 0, 1, 2, \dots). \end{aligned} \quad (41)$$

2) 反对称 A-模式由此模式的尖端光滑性条件可得:

$$\text{Re}\{H(0)\} = \text{Re}\{d_1 + d_3\} = 0. \quad (42)$$

由此可得 $\left|\frac{d_1}{d_3}\right| = -\cos(\chi_0\pi)$, 则由根据连接条件 (35) 可得:

$$\frac{d_1}{d_3} = \left|\frac{d_1}{d_3}\right| e^{-i\chi_0\pi} = -\cos(\chi_0\pi) e^{-i\chi_0\pi},$$

$$\left(\chi_0 = 1 + \frac{1}{\pi} \cos^{-1} \left|\frac{d_1}{d_3}\right|\right). \quad (43)$$

因此, 此模式下的量子化条件为

$$\begin{aligned} \text{Re}\left\{\frac{1}{\sqrt{\varepsilon}}\int_0^{\rho_c}(k_0^{(1)} - k_0^{(3)})d\rho\right\} \\ = \left(2n + \frac{1}{2} + \chi_0\right)\pi \quad (n = 0, 1, 2, \dots). \end{aligned} \quad (44)$$

量子化条件 (41) 和 (44) 式确定了特征值 σ_{0n} 和相应的特征函数. 由于 $|\sigma_0| \ll 1$, 可得 (41) 和 (44) 式中积分的一个近似形式, 从而简化这两个色散关系. 从方程 (17) 可以得到波数函数 k_e 在 $\sigma_0 \rightarrow 0$ 极限过程中有如下渐近展开:

$$\begin{aligned} k_e^{(3)} &= i(\rho - i)\sigma_e + \dots, \\ k_e^{(1)} &= e^{\frac{5}{4}\pi i}(\rho - i)^{\frac{1}{4}}(\rho + i)^{\frac{3}{4}} \\ &\quad - \frac{i}{2}(\rho - i)\sigma_e + \dots, \end{aligned} \quad (45)$$

则有

$$\begin{aligned} k_0^{(1)} - k_0^{(3)} \\ = \frac{2(1 - \lambda_0)\sqrt{\bar{A}_1}}{\pi\sqrt{1 - \alpha_4 B_0}} \left[e^{\frac{5}{4}\pi i} \frac{(\rho - i)^{\frac{1}{4}}(\rho + i)^{\frac{3}{4}}}{(\rho + ia)(\rho - ia)} \right. \\ \left. - \frac{3i}{2} \frac{(\rho - i)}{(\rho + ia)(\rho - ia)} \sigma_e + \dots \right], \end{aligned} \quad (46)$$

当 $\sigma_e = 0$ 时, 则 $\sqrt{1 - \alpha_4 B_0}$ 为确定常数. 由方程 (46) 可以得到

$$\begin{aligned} \int_0^{\rho_c} [k_0^{(1)} - k_0^{(3)}]d\rho \\ = \left(\int_0^{-i(a-0)} + \int_{\delta_r} + \int_{-i(a+0)}^{-i} + \int_{-i}^{\rho_c} \right) \\ \times [k_0^{(1)} - k_0^{(3)}]d\rho, \end{aligned} \quad (47)$$

这里 δ_r 是一个中心在 $\rho = -ia$ 连接点 $\rho = -i(a-0)$ 和 $\rho = -i(a+0)$ 的半圆, 沿顺时针方向. 由公式 $C : z = z(t), \alpha < t < \beta$ 时, 有 $\int_C^f(z)dz =$

$\int_\alpha^\beta f(z(t))z'(t)dt$. 则有:

$$\begin{aligned} \text{Re}\left\{\int_0^{\rho_c}[k_0^{(1)} - k_0^{(3)}]d\rho\right\} \\ = \frac{\sqrt{\bar{A}_1}}{\sqrt{1 - \alpha_4 B_0}} \left[(2\lambda_0 - 1)^{\frac{3}{4}} - \frac{3}{2}\sigma_e \right]. \end{aligned} \quad (48)$$

则可以得到简化的量子化条件:

S-模式

$$\begin{aligned} \frac{3}{2}\sigma_e &= (2\lambda_0 - 1)^{\frac{3}{4}} - \sqrt{\frac{\varepsilon(1 - \alpha_4 B_0)}{\bar{A}_1}} \\ &\quad \times (2n \pm 1/2)\pi; \end{aligned} \quad (49)$$

A-模式

$$\frac{3}{2}\sigma_e = (2\lambda_0 - 1)^{\frac{3}{4}} - \sqrt{\frac{\varepsilon(1 - \alpha_4 B_0)}{\hat{A}_1}} \times \left(2n + \frac{1}{2} + \chi_0\right)\pi. \quad (50)$$

对给定的 λ_0 , 系统允许一组中性稳定模式 $\sigma_{0n} = 0$, 此时 $\varepsilon = \varepsilon_n (n = 0, 1, 2)$. 发现含有各向异性表面张力时, 对于同一个 n , LF-S 模式比 LF-A 模式更危险. 代入 ε_c 和 \hat{A}_1 后, 由 LF-S 的方程 (49), 可得 ε 与 λ_0 在中性稳定模式下的关系式为

$$\varepsilon = \left(\frac{2\varepsilon_c}{\pi}\right)^{\frac{1}{2}} (2\lambda_0 - 1)^{\frac{3}{8}} \left(\frac{\hat{A}_1}{1 - \alpha_4 B_0}\right)^{\frac{1}{4}}. \quad (51)$$

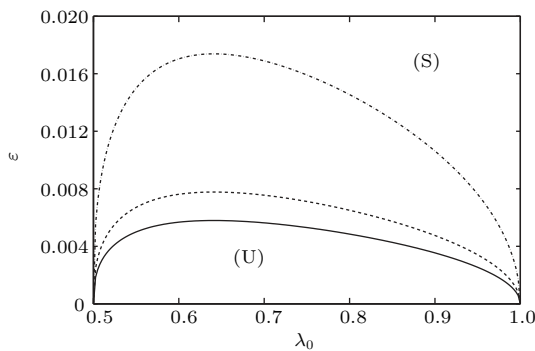


图3 LF-S 中性模式曲线 从上到下三条曲线分别对应 $n = 0, 1, 2$; 各参数值为 $\varepsilon_c = 0.5388 \times 10^{-2}$, $M = 0.09552$, $\kappa = 0.29$, $G_c = 0.11485 \times 10^{-4}$, $\lambda_G = 0.4989$, $\alpha_4 = 0.1$

Fig. 3. The neutral curves of the LF-S-modes for the case $\varepsilon_c = 0.5388 \times 10^{-2}$, $M = 0.09552$, $\kappa = 0.29$, $G_c = 0.11485 \times 10^{-4}$, $\lambda_G = 0.4989$, $\alpha_4 = 0.1$, and $n = 0, 1, 2$ from top to bottom.

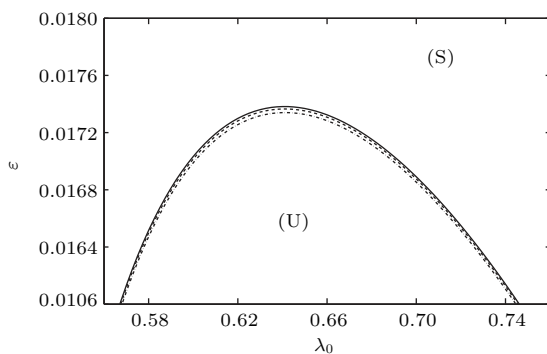


图4 LF-S 中性模式曲线 ($n = 0$) 各参数值为 $\varepsilon_c = 0.5388 \times 10^{-2}$, $M = 0.09552$, $\kappa = 0.29$, $G_c = 0.11485 \times 10^{-4}$, $\lambda_G = 0.4989$, 从下到上的三条曲线分别对应 $\alpha_4 = 0, 0.06, 0.1$

Fig. 4. The neutral curves of the LF-S-modes ($n = 0$) for the case $\varepsilon_c = 0.5388 \times 10^{-2}$, $M = 0.09552$, $\kappa = 0.29$, $G_c = 0.11485 \times 10^{-4}$, $\lambda_G = 0.4989$, and $\alpha_4 = 0, 0.06, 0.1$ from bottom to top.

由 (51) 可以得到 ε_* 与 λ_0 的关系, 由图 3 可得在 LF 机制下最危险的模式为 $n = 0$ 的模式. 由图 4 可得, 当各向异性表面张力参数 α_4 越大时, 系统就越不稳定.

从上述分析可得, LF-S 中性模式产生弱振荡的胞晶结构 [10], 将参数平面 (ε, λ_0) 分成了两个区域, (S) 区域 (稳定区域) 和 (U) 区域 (不稳定区域). 系统的基态服从振荡稳定性判据: $(\varepsilon, \lambda_0) \in (S)$, 稳定; $(\varepsilon, \lambda_0) \in (U)$, 不稳定.

7 结 论

本文研究了定向凝固过程中表面张力为各向异性的深胞晶界面形态的稳定性机制. 应用匹配渐近展开法和多重变量渐近展开法解决了表面张力为各向异性时线性绕动态的特征值问题, 得到了整体模式解以及相应特征值的量子化条件. 发现各向异性表面张力对定向凝固系统中包含的两种整体不稳定性机制: 整体波动不稳定性 and 低频不稳定性都有影响. 在中性模式产生强振荡的枝晶结构的整体波动不稳定性 GTW 中, GTW-S 模式 $n = 0$ 是最危险的振荡模式; 而在中性模式产生弱振荡的胞晶结构的低频不稳定性 LF 中, LF-S 模式 $n = 0$ 是最危险的弱振荡模式. 并且随着各向异性表面张力的增加, 整体波动不稳定性的不稳定区域减小; 而低频不稳定性的不稳定区域增加.

参考文献

- [1] Mullins W W, Sekerka R F 1963 *J. Appl. Phys.* **34** 323
- [2] Mullins W W, Sekerka R F 1964 *J. Appl. Phys.* **35** 444
- [3] Pelcé P, Pumir A 1985 *J. Cryst. Growth* **73** 337
- [4] Karma A, Pelcé P 1990 *Phys. Rev. A* **41** 4507
- [5] Pocheau A, Georgelin M 2003 *J. Cryst. Growth* **250** 100
- [6] Georgelin M, Pocheau A 2004 *J. Cryst. Growth* **268** 272
- [7] Georgelin M, Pocheau A 2006 *Phys. Rev. E* **73** 011604
- [8] Georgelin M, Pocheau A 2009 *Phys. Rev. E* **81** 031601
- [9] Chen Y Q, Xu J J 2011 *Phys. Rev. E* **83** 041601
- [10] Xu J J, Chen Y Q 2011 *Phys. Rev. E* **83** 061605
- [11] Saffman P G, Taylor G I 1958 *Proc. R. Soc. London A* **245** 312
- [12] Wang Z J, Wang J C, Yang G C 2008 *Acta Phys. Sin.* **57** 1246 (in Chinese) [王志军, 王锦程, 杨根仓 2008 物理学报 **57** 1246]
- [13] Wang Z J, Wang J C, Yang G C 2010 *Chin. Phys. B* **19** 017305
- [14] Chen M W, Chen Y C, Zhang W L, Liu X M, Wang Z D 2014 *Acta Phys. Sin.* **63** 038101 (in Chinese) [陈明文, 陈奕臣, 张文龙, 刘秀敏, 王自东 2014 物理学报 **63** 038101]

Effect of surface tension anisotropy on the interface morphological stability of deep cellular crystal

Jiang Han¹⁾ Chen Ming-Wen^{2)†} Shi Guo-Dong¹⁾ Wang Tao¹⁾ Wang Zi-Dong^{1)‡}

1) (*School of Materials Science and Engineering, University of Science and Technology Beijing, Beijing 100083, China*)

2) (*School of Mathematics and Physics, University of Science and Technology Beijing, Beijing 100083, China*)

(Received 7 January 2016; revised manuscript received 1 February 2016)

Abstract

In this paper, we study the effect of anisotropic surface tension on the interface morphological stability of deep cellular crystal during directional solidification. We assume that the process of solidification is viewed as a two-dimensional problem, the anisotropic surface tension is a four-fold symmetry function, the solute diffusion in the solid phase is negligible, the thermodynamic properties are the same for both solid and liquid phases, and there is no convection in the system. On the basis of the basic state solution for the deep cellular crystal in directional solidification, by the matched asymptotic expansion method and the multiple variable expansion method, we obtain the asymptotic solution, and then the quantization condition of interfacial morphology for deep cellular crystal is obtained.

The results show that by comparison with the directional solidification system of surface tension isotropy, the interface morphological stability of surface tension anisotropy also possesses two types of global instability mechanisms: the global oscillatory instability (GTW-mode), whose neutral modes yield strong oscillatory dendritic structures, and the low-frequency instability (IF-mode), whose neutral modes yield weakly oscillatory cellular structures. Both of the two global instability mechanisms have the symmetrical mode (S-mode) and the anti-symmetrical mode (A-mode), and the growth rate of the S-mode with the same index n is greater than that of the A-mode. In this sense we say that the S-mode is more dangerous than the A-mode. All the neutral curves of the GTW-S-modes and LF-S-modes divide the parameter plane into two subdomains: the stable domain and the unstable domain. In the paper we show the neural curves of the GTW-S-modes and LS-S-modes for various n , respectively. It is seen that among all the GTW-S-modes ($n = 0, 1, 2$), the GTW-S-mode with $n = 0$ is the most dangerous oscillatory mode, while among all the LF-S-modes ($n = 0, 1, 2$), the LF-S-mode with $n = 0$ is the most dangerous weakly oscillatory mode. We also show the neural curves of the GTW-S-mode ($n = 0$) and LS-S-mode ($n = 0$) for various anisotropic surface tension parameters, respectively. It is seen that as the anisotropic surface tension increases, the unstable domain of global oscillatory instability decreases, and the unstable domain of the low-frequency instability increases.

Keywords: directional solidification, anisotropic surface tension, deep cellular crystal growth, global instabilities

PACS: 68.70.+w, 81.10.Aj, 81.30.Fb

DOI: 10.7498/aps.65.096803

† Corresponding author. E-mail: chenmw@ustb.edu.cn

‡ Corresponding author. E-mail: wangzidong64@126.com